Supplementary information

Two-dimensional transition metal diborides: promising Dirac electrocatalysts with large reaction regions toward efficient N_2 fixation

Xuemin Hu,[a] Shiying Guo,[b] Shengli Zhang,*[b] Xiangyu Guo,[c] Yafei Li[d], Shiping Huang,[c] Kan Zhang[b] and Junwu Zhu*[a]

[a]Key Laboratory for Soft Chemistry and Functional Materials, Ministry of Education, Nanjing University of Science and Technology, Nanjing 210094, China

[b]MIIT Key Laboratory of Advanced Display Materials and Devices, School of Materials Science and Engineering, Nanjing University of Science and Technology, Nanjing 210094, China

[c]State Key Laboratory of Organic-Inorganic Composites, Beijing University of Chemical Technology, Beijing 100029, China

[d]Jiangsu Key Laboratory of New Power Batteries, Jiangsu Collaborative Innovation Centre of Biomedical Functional Materials, School of Chemistry and Materials Science, Nanjing Normal University, Nanjing 210023, China

*Corresponding author E-mail: zhangslvip@njust.edu.cn, zhujw@njust.edu.cn

Table S1. The optimized lattice constants (*a*, *b*), buckling height, B-B and M-B bond lengths, Bader charge of transition metals, cohesive energies of TiB_2 and NbB_2 monolayers.

Table S2. Effective independent elastic constants (C_{ij}, N/m), Young's modulus (E, N/m), and Poisson's ratio (v) of TiB_2 and NbB_2 monolayers.

Table S3. Computed adsorption energies (E_{ad}, eV) of N_2 on boron and transition metal surfaces of TiB_2 and NbB_2 monolayers by end-on and side-on way.

Table S4. Computed zero-point energies (E_{ZPE}, eV) and entropy at T=298.15 K (TS, eV) of different adsorption species for each adsorption species for TiB_2 and NbB_2 monolayers, which are obtained from the vibrational frequency calculations.

Table S5. Computed electronic energies (ΔE, eV) and Gibbs free energies (ΔG, eV) for each reaction steps

Table S6. Optimized N-N bond lengths (Å) during the NRR on TiB_2 and NbB_2 monolayers.

Fig. S1. Phonon spectra of (a) TiB_2 and (b) NbB_2 monolayers.

Fig. S2. Schematic diagrams of density of states around Fermi level for (a) TiB_2 and (b) NbB_2 monolayers.

Fig. S3. The band structures based on HSE06 functional of (a) TiB_2 and (b) NbB_2 monolayers.

Fig. S4. Variations of the DFT energy of (a) TiB_2 and (b) NbB_2 monolayer from 0 to 5 ps during ab initio molecular dynamics (AIMD) simulations at the temperature of 300 K under H_2O and N_2 atmosphere. (c-d) Snapshot of atomic configuration of AIMD simulations for NbB_2 monolayer. (c) is the initial structure, and (d) is the final structure after 5 ps. The model we use here includes a 4 × 4 × 1 TiB_2/NbB_2 supercell, 4 N_2 molecules, and 9 H_2O molecules. Green, blue, orange atoms are N, O, H, respectively. Gray and pink atoms represent Nb and B.

Fig. S5. (a) The adsorption energies between TMs and O/H atoms of H_2O/N_2 on the TM side of 2D TiB_2 and NbB_2 monolayers. (b-d) The atomic structures of H_2O and N_2 adsorbed on the TM side of 2D TiB_2 and NbB_2 monolayers.

Fig. S6. The charge variations of the $*N_xH_y$ during the NRR steps for (a) TiB_2 and (b)

NbB_2 monolayers.

Fig. S7. Charge density difference of (a-c) N_2-TiB_2 and (d-f) N_2-NbB_2 systems. The isosurface value is set to 0.003 e/Bohr^3. The yellow and cyan regions represent positive and negative charges, respectively.

Fig. S8. The kinetic barriers of key steps and corresponding atomic configurations of initial states (IS), transitional states (TS), final states (FS) for NRR and HER on TiB_2 (a-b) and NbB_2 (c-d) monolayers.

Table S1. The optimized lattice constants (*a*, *b*), buckling height, B-B and M-B bond lengths, Bader charge of transition metals, cohesive energies of TiB_2 and NbB_2 monolayers.

MB_2	*a*=*b* (Å)	Height (Å)	B-B(Å)	M-B(Å)	Ti/Nb	E_{coh} (eV/atom)
TiB_2	3.13	1.20	1.81	2.17	1.16	-6.49
NbB_2	2.96	1.65	1.71	2.38	0.69	-7.23

Table S2. Effective independent elastic constants (C_{ij}, N/m), Young's modulus (*E*, N/m), and Poisson's ratio (*v*) of TiB_2 and NbB_2 monolayers.

MB_2	C_{11}	C_{22}	C_{12}	C_{44}	*E*	*v*
TiB_2	165.14	165.14	-8.12	86.63	164.74	-0.05
NbB_2	184.61	184.61	11.12	86.75	183.94	0.06

Table S3. Computed adsorption energies (E_{ad}, eV) of N_2 on boron and transition metal surfaces of TiB_2 and NbB_2 monolayers by end-on and side-on way.

TiB_2	Adsorption way	E_{ad}	NbB_2	Adsorption way	E_{ad}
B-surface	end-on	-0.11	B-surface	end-on	-0.18
	side-on	-0.05		side-on	-0.18
Ti-surface	end-on	-0.09	Nb-surface	end-on	-1.09
	side-on	-2.54		side-on	-3.13

Table S4. Computed zero-point energies (E_{ZPE}, eV) and entropy at T=298.15 K (TS, eV) of different adsorption species for each adsorption species for TiB_2 and NbB_2 monolayers, which are obtained from the vibrational frequency calculations.

TiB_2		NbB_2	
Adsorption Species	E_{ZPE}-TS	Adsorption Species	E_{ZPE}-TS
$*N_2$	0.17	$*N_2$	0.17
$*N_2H$	0.47	$*N_2H$	0.47
$*N_2H_2$	0.76	$*N_2H_2$	0.74
$*N_2H_3$	1.09	$*N_2H_3$	0.94
$*N_2H_4$	1.25	$*N_2H_4$	1.21
*NH	0.34	$*N_2H_5$	1.52
$*NH_2$	0.54	$*NH_2$	0.57
$*NH_3$	0.91	$*NH_3$	0.93

Table S5. Computed electronic energies (ΔE, eV) and Gibbs free energies (ΔG, eV) for each reaction steps

TiB_2			NbB_2		
Adsorption Species	ΔE	ΔG	Adsorption Species	ΔE	ΔG
$*\rightarrow*N_2$	-2.54	-1.99	$*\rightarrow*N_2$	-3.13	-2.58
$*N_2\rightarrow*N_2H$	-0.17	0.17	$*N_2\rightarrow*N_2H$	-0.31	0.03
$*N_2H\rightarrow*N_2H_2$	-0.1	0.32	$*N_2H\rightarrow*N_2H_2$	0.04	0.35
$*N_2H_2\rightarrow*N_2H_3$	0.18	0.55	$*N_2H_2\rightarrow*N_2H_3$	-2.44	-2.20
$*N_2H_3\rightarrow*N_2H_4$	-2.41	-2.21	$*N_2H_3\rightarrow*N_2H_4$	0.25	0.55
$*N_2H_4\rightarrow*NH$	1.28	0.76	$*N_2H_4\rightarrow*N_2H_5$	0.27	0.62
$*NH\rightarrow*NH_2$	0.20	0.44	$*N_2H_5\rightarrow*NH_2$	1.40	0.84
$*NH_2\rightarrow*NH_3$	0.17	0.58	$*NH_2\rightarrow*NH_3$	0.24	0.64
$*NH_3\rightarrow*$	0.82	0.33	$*NH_3\rightarrow*$	1.32	0.78

Table S6. Optimized N-N bond lengths (Å) during the NRR on TiB_2 and NbB_2 monolayers.

MB_2	N≡N	$*N_2$	$*N_2H$	$*N_2H_2$	$*N_2H_3$	$*N_2H_4$
TiB_2	1.123	1.337	1.415	1.473	1.471	3.498
NbB_2	1.123	1.339	1.403	1.461	3.167	/

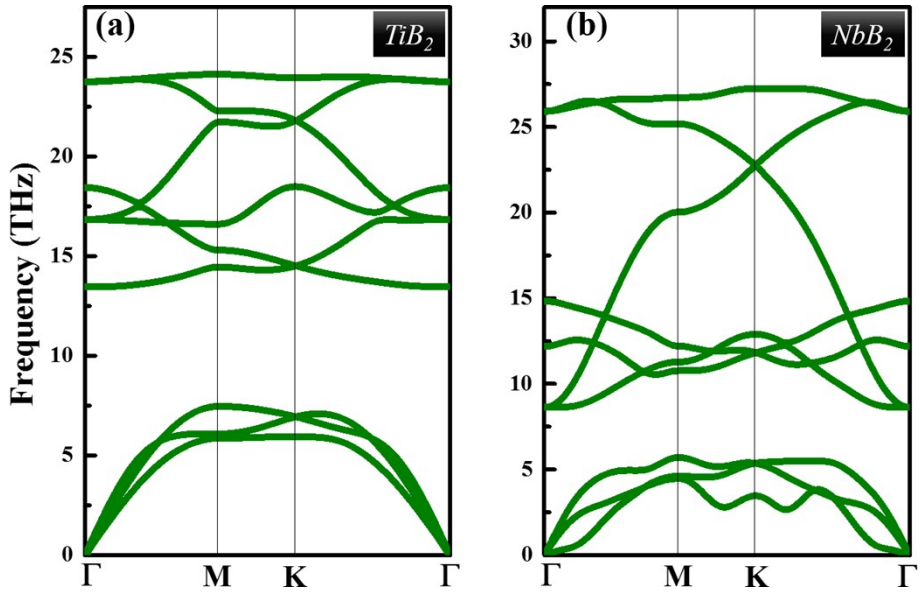

Fig. S1. Phonon spectra of (a) TiB_2 and (b) NbB_2 monolayers.

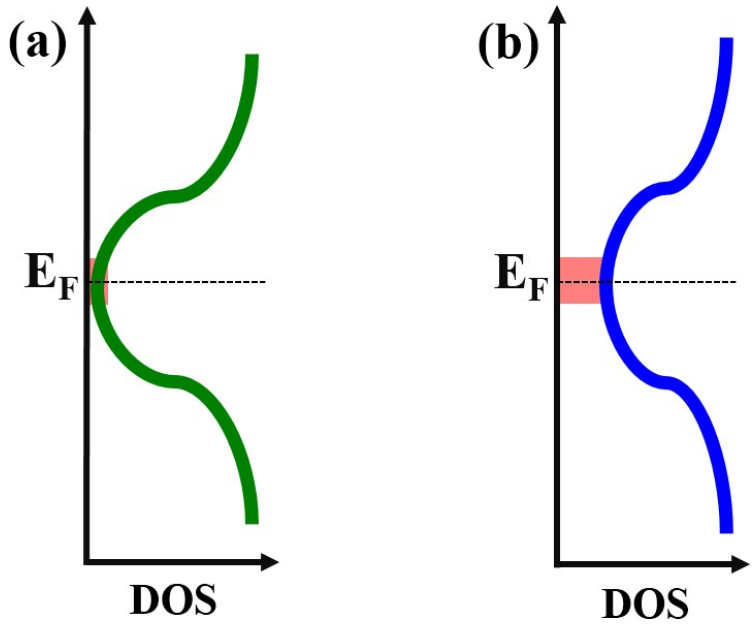

Fig. S2. Schematic diagrams of density of states around Fermi level for (a) TiB_2 and (b) NbB_2 monolayers.

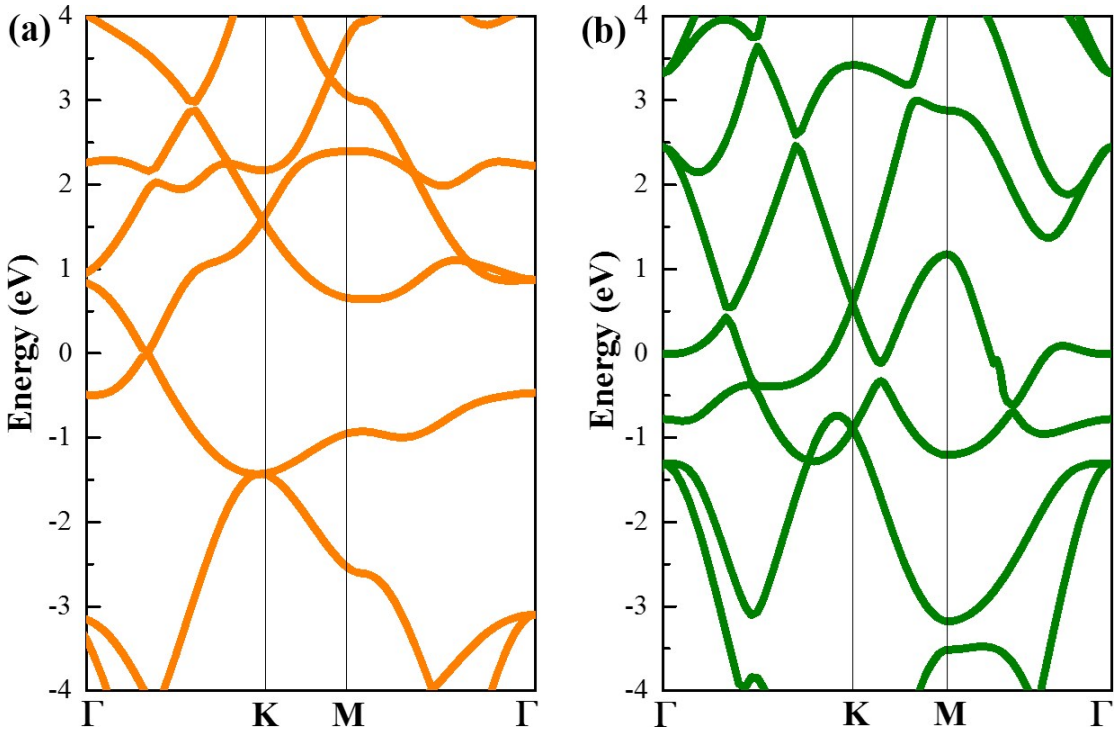

Fig. S3. The band structures based on HSE06 functional of (a) TiB_2 and (b) NbB_2 monolayers.

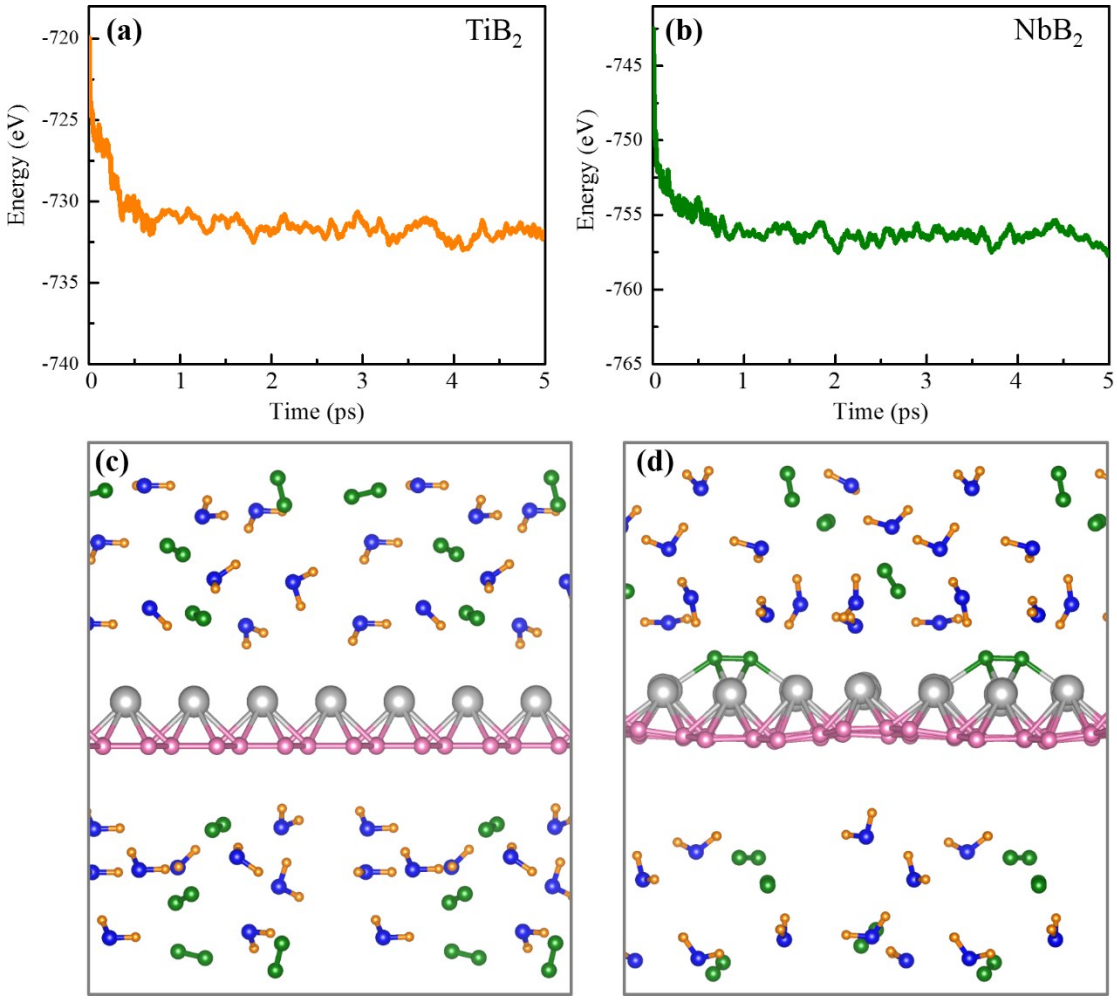

Fig. S4. Variations of the DFT energy of (a) TiB_2 and (b) NbB_2 monolayer from 0 to 5 ps during ab initio molecular dynamics (AIMD) simulations at the temperature of 300 K under H_2O and N_2 atmosphere. (c-d) Snapshot of atomic configuration of AIMD simulations for NbB_2 monolayer. (c) is the initial structure, and (d) is the final structure after 5 ps. The model we use here includes a 4 × 4 × 1 TiB_2/NbB_2 supercell, 4 N_2 molecules, and 9 H_2O molecules. Green, blue, orange atoms are N, O, H, respectively. Gray and pink atoms represent Nb and B.

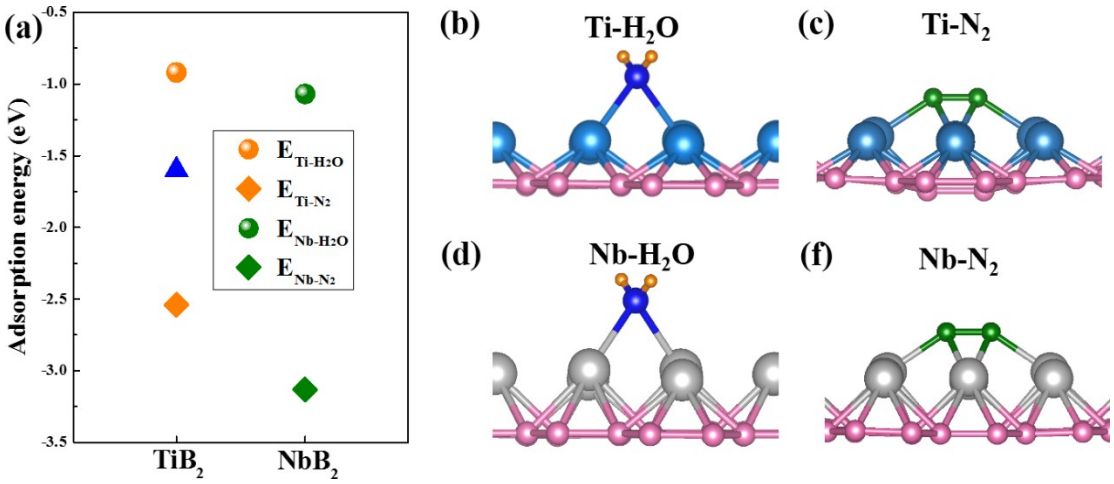

Fig. S5. (a) The adsorption energies between TMs and O/H atoms of H_2O/N_2 on the TM side of 2D TiB_2 and NbB_2 monolayers. (b-d) The atomic structures of H_2O and N_2 adsorbed on the TM side of 2D TiB_2 and NbB_2 monolayers.

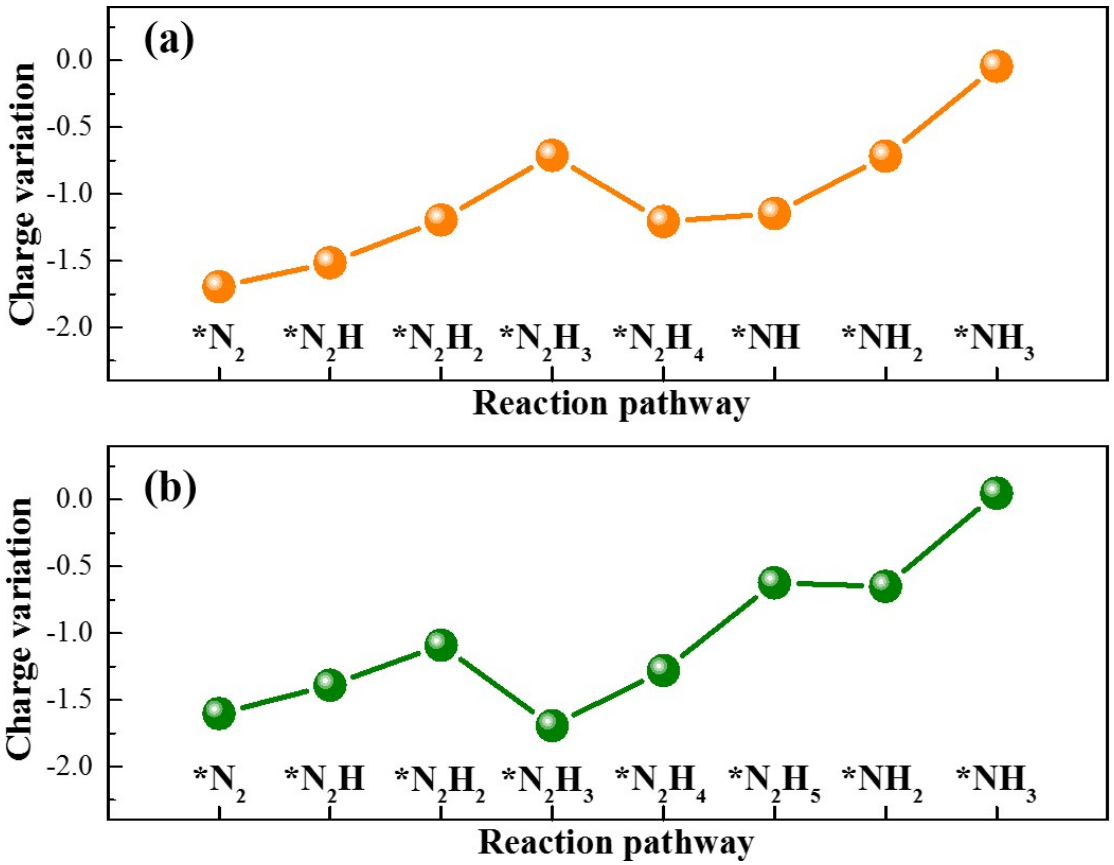

Fig. S6. The charge variations of the $*N_xH_y$ during the NRR steps for (a) TiB_2 and (b) NbB_2 monolayers.

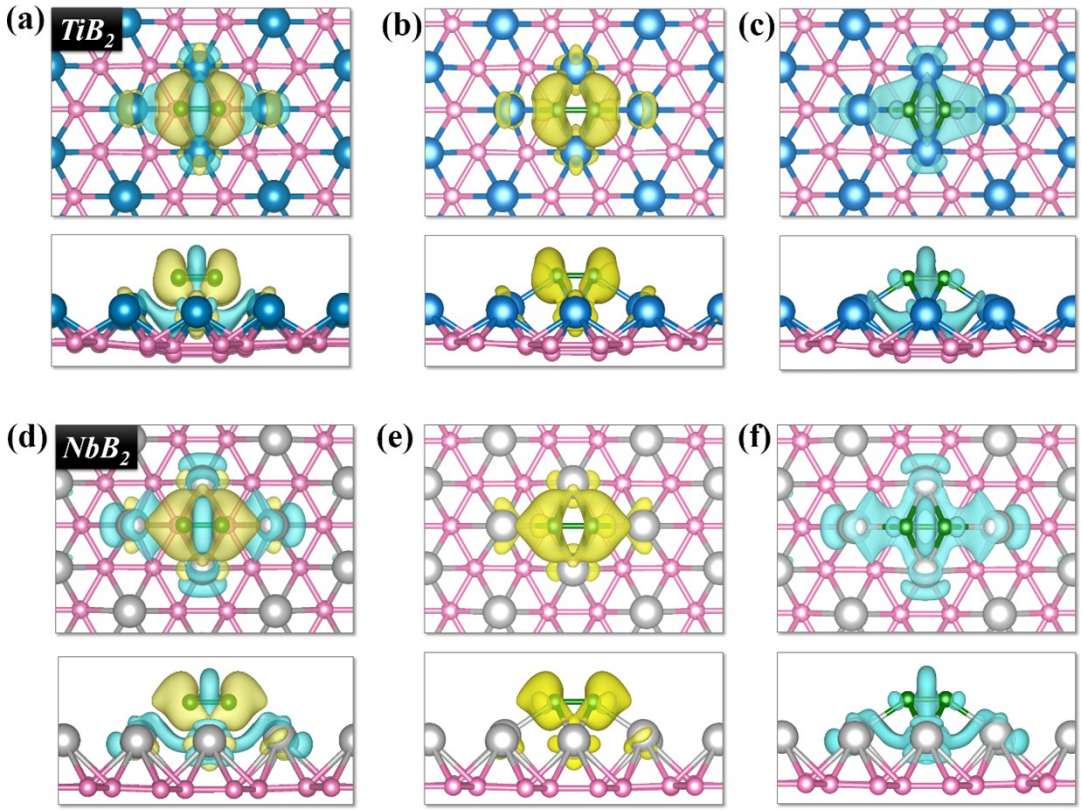

Fig. S7. Charge density difference of (a-c) N_2-TiB_2 and (d-f) N_2-NbB_2 systems. The isosurface value is set to 0.003 e/Bohr^3. The yellow and cyan regions represent positive and negative charges, respectively.

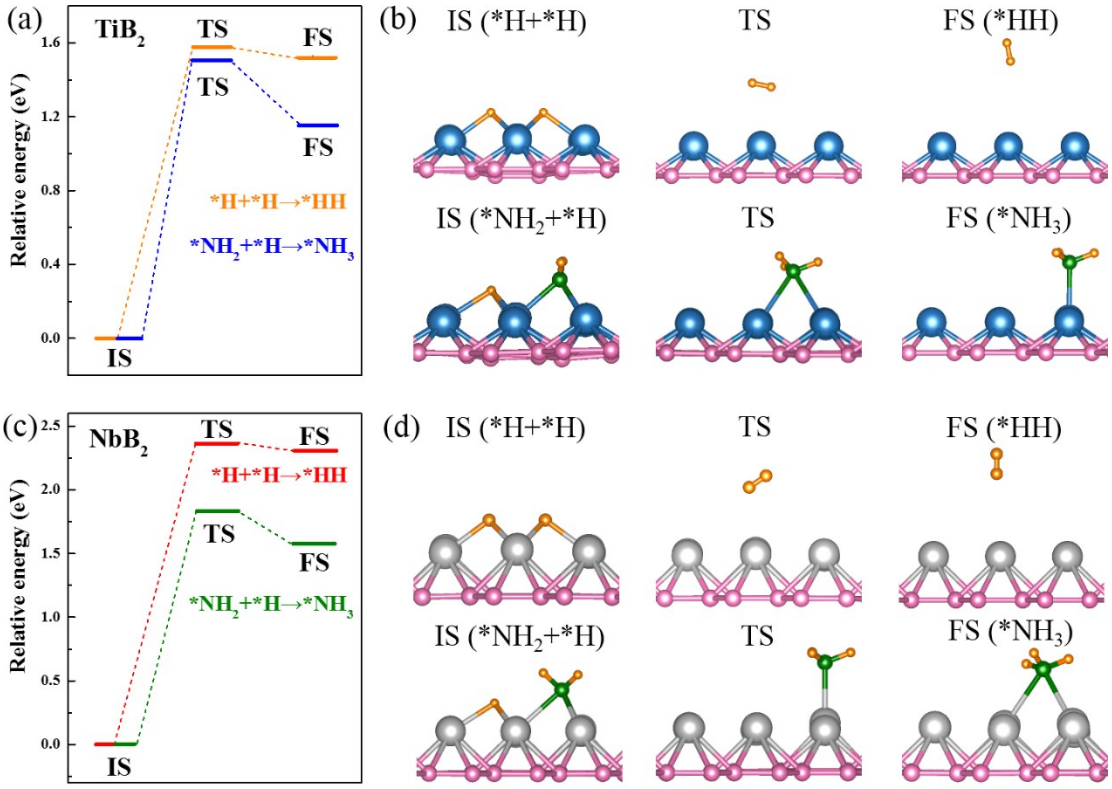

Fig. S8. The kinetic barriers of key steps and corresponding atomic configurations of initial states (IS), transitional states (TS), final states (FS) for NRR and HER on TiB_2 (a-b) and NbB_2 (c-d) monolayers.